AFRL-DE
TR-2001-1015

COST EFFECTIVE, SCALABLE OPTICALLY PUMPED MOLECULAR LASER

Jeff Nicholson and David Neumann

Directed Energy Solutions
14125 Candlewood Ct
Colorado Springs, CO 80921

And

Wolfgang Rudolph

Department of Physics and Astronomy
University of New Mexico
Albuquerque, NM 87131

February 2001

Final Report

AIR FORCE RESEARCH LABORATORY
Directed Energy Directorate
3550 Aberdeen Ave SE
AIR FORCE MATERIEL COMMAND
KIRTLAND AIR FORCE BASE, NM 87117-5776

AFRL-DE-TR-2001-1015

Using Government drawings, specifications, or other data included in this document for any purpose other than Government procurement does not in any way obligate the U.S. Government. The fact that the Government formulated or supplied the drawings, specifications, or other data, does not license the holder or any other person or corporation; or convey any rights or permission to manufacture, use, or sell any patented invention that may relate to them.

This report has been reviewed by the Public Affairs Office and is releasable to the National Technical Information Service (NTIS). At NTIS, it will be available to the general public, including foreign nationals.

If you change your address, wish to be removed from this mailing list, or your organization no longer employs the addressee, please notify AFRL/DELC, 3550 Aberdeen Ave SE, Kirtland AFB, NM 87117-5776.

Do not return copies of this report unless contractual obligations or notice on a specific document requires its return.

This report has been approved for publication.

GORDON D. HAGER, DR-IV, DAF,
Project Manager

FOR THE COMMANDER

JOHN C. DEL BARGA, MAJ, USAF
Chief, High Power Gas Lasers Branch

DR. EARL GOOD, SES
Director, Directed Energy Directorate

REPORT DOCUMENTATION PAGE

Form Approved
OMB No. 0704-0188

1. REPORT DATE (DD-MM-YYYY)	2. REPORT TYPE	3. DATES COVERED (From - To)
28-02-2001	Final Report	01-05-00 to 28-01-01

4. TITLE AND SUBTITLE
Cost Effective, Scalable Optically Pumped Molecular Laser

5a. CONTRACT NUMBER
F29601-00-C-0095

5b. GRANT NUMBER

5c. PROGRAM ELEMENT NUMBER
65502F

6. AUTHOR(S)
Jeff Nicholson, David Neumann, and Wolfgang Rudolph*

5d. PROJECT NUMBER
3005

5e. TASK NUMBER
DO

5f. WORK UNIT NUMBER
DX

7. PERFORMING ORGANIZATION NAME(S) AND ADDRESS(ES)

Directed Energy Solutions
14125 Candlewood Ct.
Colorado Springs, CO 80921

8. PERFORMING ORGANIZATION REPORT NUMBER

DES2001-02

9. SPONSORING / MONITORING AGENCY NAME(S) AND ADDRESS(ES)
Air Force Research Laboratory
Directed Energy Directorate
3550 Aberdeen Ave SE
Kirtland AFB NM 87117-5776

10. SPONSOR/MONITOR'S ACRONYM(S)

11. SPONSOR/MONITOR'S REPORT NUMBER(S)
AFRL-DE-TR-2001-1015

12. DISTRIBUTION / AVAILABILITY STATEMENT

Approved for public release; distribution is unlimited

13. SUPPLEMENTARY NOTES

*University of New Mexico
Scholes Hall 102
Albuquerque, NM 87131-6003

14. ABSTRACT

Report developed under SBIR contract for topic AF00-023. An optically pumped, HBr laser was demonstrated operating at 4.0 μm. This is the first demonstration of an HBr laser by direct optical pumping of the 0 → 3 vibrational overtone band at 1.34 μm. An injection locked, temperature tuned Nd: YAG laser was used as the optical pump source. Lasing was achieved in a cell of HRr maintained at 100 Torr. Potential for scaling to higher pulse energies has been demonstrated. The HBr laser has potential use as a source for infrared countermeasures.

15. SUBJECT TERMS
HBr, Hydrogen Bromide, Optically Pumped, Molecular Laser

16. SECURITY CLASSIFICATION OF:			17. LIMITATION OF ABSTRACT	18. NUMBER OF PAGES	19a. NAME OF RESPONSIBLE PERSON
a. REPORT	b. ABSTRACT	c. THIS PAGE			Dr. Gordon Hager
Unclassified	Unclassified	Unclassified	UL	32	19b. TELEPHONE NUMBER (include area code) (505) 853-0574

Table of Contents

FIGURES

Cost-Effective, Scalable Optically Pumped Molecular Lasers (OPML)

Final Phase 1 Report, Contract No. F29601-00-C-0095

1.0 Summary

The v = 0 →3 transition of HBr has been successfully pumped by an injection seeded, Nd:YAG laser operating at 1.3391 μm with subsequent laser oscillation at 4 μm. In performing this task, our Phase I program has focused on demonstrating the important physical principles associated with this process. These include the ability to narrow-band, frequency shift and control the pump source and the ability to efficiently couple pump energy into the lasing species. As such, the critical techniques for narrow-lining the optical source, temperature tuning and stabilizing the output frequency of the optical source; efficient coupling of optical energy into the molecular laser; and efficient optical extraction from the lasing molecule have been demonstrated. In addition, work to date has concentrated on high-resolution spectroscopy of the HBr and Nd:YAG laser to ensure that the pump source can be made to overlap an HBr absorption.

The Nd:YAG is forced to operate in the 1.3 μm region with dielectric mirrors that have a high reflectivity at 1.3 μm and low reflectivity at 1.064 μm. Course frequency tuning of the Nd:YAG is provided through temperature control of the YAG rod. The 1.34 μm line is selected through the use of intracavity etalons, and fine frequency control/ bandwidth narrowing is provided by injection seeding from a narrow linewidth tunable diode laser.

The important parameter of demonstrating efficient and scalable lasing will be demonstrated in a follow-on SBIR Phase II program. To date, there have not been any effects discovered which would significantly limit scaling to higher powers. An added part of our work has dealt with examining other potential high-power OPML candidates. In particular we examined molecular iodine and find it to have great potential as a high power OPML for a multitude of DOD missions. The greater potential of molecular iodine for meeting a variety of Air Force needs and the investor support has encouraged making this a complementary candidate to HBr in the follow-on Phase II program. The following sections summarize the results obtained in this Phase I contract.

2.0 Introduction

2.1 Optically Pumped Molecular Lasers (OPML)

Electrically powered, diode and fiber laser pumped, molecular gas lasers are proposed for a wide variety of important military missions. The important advantages that these laser concepts offer include superior beam quality, efficiency, wavelength diversity, and a wide range of power scaling making them useful for a variety of Air Force missions. In this approach, molecular gases are optically excited by well-developed, highly efficient optical sources such as solid-state lasers, laser diodes or doubled fiber lasers. The laser gas medium can effectively act as a beam-combining medium, where it combines numerous pump apertures into a single coherent beam. This single feature is the key to scaling laser devices to much higher powers than the semiconductor or solid state approaches alone. Several approaches exist: pumping the lasing molecule directly (the method employed here), pumping a long-lived, storage molecule, which transfers its energy to a lasing species or pumping a molecule to a dissociative state which yields an atom in a state of inversion.

The HBr molecule is a promising candidate species for high power Optically Pumped Molecular Laser (OPML) applications because its fundamental vibrational transition lies in the 3.9 to 4.1 μm region, which overlaps a narrow atmospheric transmission window. Figure 1 shows the results of a HiTran calculation of atmospheric propagation and illustrates the narrow region of high transmission where the HBr laser would operate.

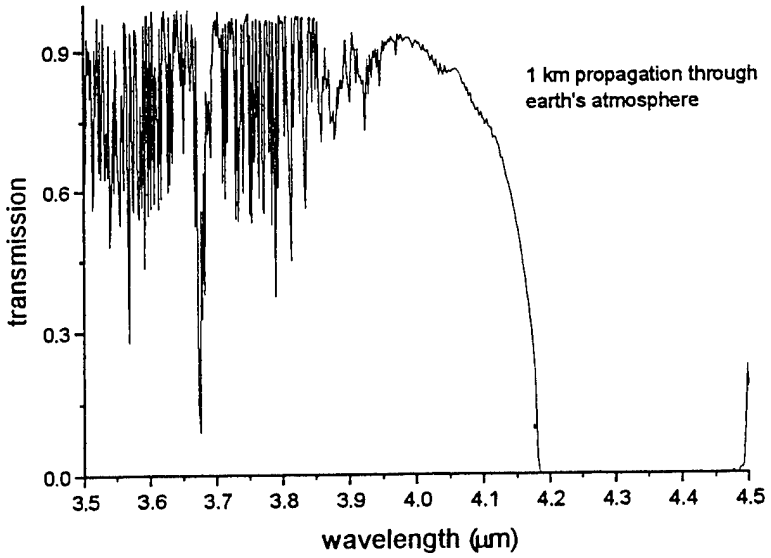

Figure 1: Transmission in the atmosphere in the 4 μm region.

Furthermore, the narrow HBr ($v = 0 \rightarrow v = 3$) overtone absorption lies in the 1.3 μm region, which makes optical pumping of HBr by high power Nd:YAG laser a strong prospect. In this manner, we propose the development of an HBr laser pumped on the 0-3 vibrational overtone by a Nd:YAG laser.

Although diode and fiber laser pumped molecular gas lasers in general, and the HBr laser in particular, have not received appreciable attention within DoD, there appear to be a number of compelling reasons for developing this technology:

a. Very rapid advances in power scaling should be expected because of the use of proven diode/fiber laser and gas laser technologies.
b. A large portion of the investment needed to scale these devices to high power will be paid for by commercial industry because of their significant investment in the rapidly expanding market for solid-state, diode and fiber laser systems.
c. Wavelength agile, highly efficient systems are envisioned which can offer substantial advantages for applications in the mid infrared.
d. There would be immediate pay-off in commercial applications in the communication and materials processing industries.

Our novel approach to combining solid state/diode/fiber laser with molecular laser technology can lead to the next generation of medium and high power mid infrared lasers.

2.2 Physical Properties of HBr Lasing

The physical and chemical properties of HBr are well known and thus lend it to facile lasing in the 4 micron region [1-4]. For reference, spectroscopic parameters related to HBr are collected in Table 1 in Appendix A. Figure 2 shows a simplified energy level diagram of the first four vibrational states. Each vibrational state contains a band of rotational levels. The energy spacing of two adjacent rotational levels is on the order of 500 GHz. The spectroscopic data shown in figure 2 are taken from reference [3]. The broadening of the absorption line is described by

$$\Delta\nu = \nu_0 \left(\frac{8kT \ln 2}{Mc^2} \right) \quad (1)$$

where k is Boltzmann's constant T is the gas temperature, M is the mass of HBr, c is the speed of light, and ν_0 is the frequency center of the transition. At room temperature and pressures on the order of 30 Torr, inhomogeneous broadening dominates with a FWHM of 400 MHz. The molecule occurs naturally in two isotopic forms, based on the naturally occurring ^{79}Br and ^{81}Br isotopes, with a relative abundance of 1.02 to 1.0. The resulting isotope level splitting is about 33 GHz. At room temperature only the v = 0 state is populated with the population reaching a maximum in the J=3 rotational state. Excitation of the 0-3 transition is followed by rotational relaxation (typical relaxation times at T = 300 K and p = 30 Torr are on the order of 10 ns). Lasing on adjacent vibrational levels can occur at the wavelengths shown in Figure 2. Since the rotational level spacing is much greater than the vibrational energy, dissipation is minimal and >85% of the absorbed energy can be theoretically converted to the laser output.

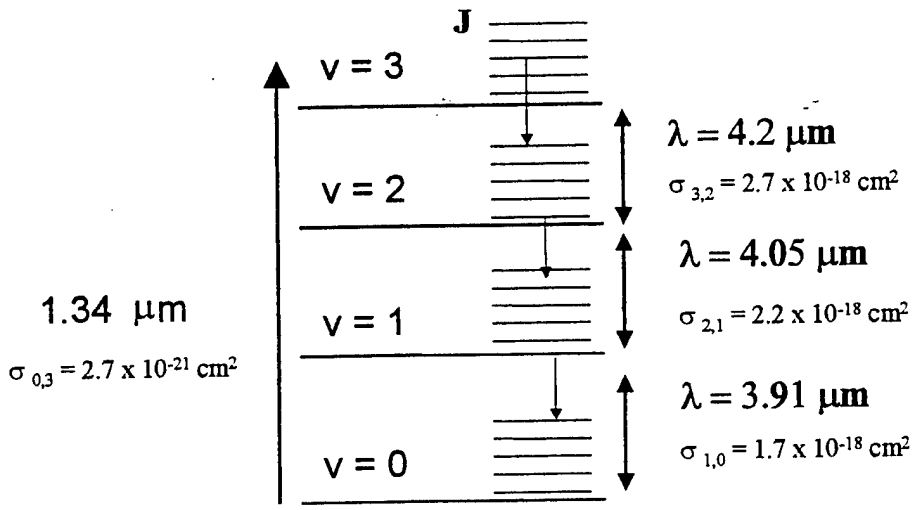

Figure 2. Simplified HBr energy levels. Shown are the first four vibrational states. The rotational levels (J) are indicated. The cross sections, σ, are from [3].

From Figure 1, the wavelength of v = 3 → 2 transition lies outside the transmission window of the atmosphere. However, the wavelengths given in Figure 2 refer to the center of the

vibrational transitions, between the R and P branch. Figure 3 shows approximate positions of the R and P branch of the $v = 3 \rightarrow 2$ transitions along with absorption due to 2 m propagation in the atmosphere. If the $J = 5$ level is populated through optical pumping of $v = 0 \rightarrow 3$, then (neglecting rotational relaxations) the R(4) and P(6) transitions would be expected to lase. However, the P transitions will be selectively absorbed by the atmosphere (primarily by CO_2). Therefore, one possibility for operating with all photons in the transmission window would be to include an intra-cavity cell of high pressure CO_2. This cell would act as a low pass wavelength filter, allowing the shorter wavelength R transitions to operate.

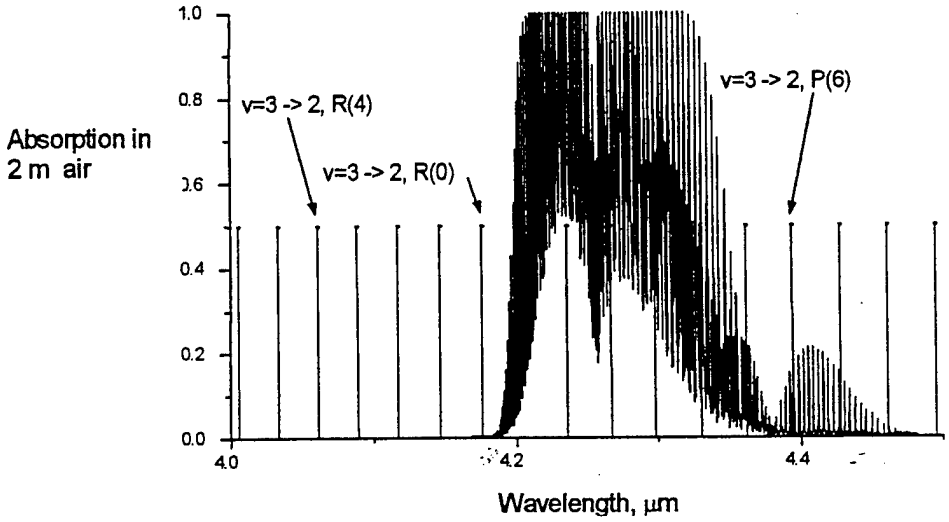

Figure 3: Approximate positions of the HBr $v = 3 \rightarrow 2$ lines are compared to absorption due to 2 m propagation in the atmosphere.

The HBr rotational linewidths are on the order of a few hundred MHz under typical operating gas pressures and are separated by approximately 0.5 THz. In order to pump HBr with a Nd:YAG laser, the wavelength of the YAG laser must be precisely controlled and operated with a narrow spectrum. Intra-cavity dispersive elements, such as a prism or etalon, were used to force the YAG to operate on a single transition. Then, temperature tuning of the YAG laser was used to move the peak of the transition as near as possible to an HBr absorption. Finally, injection seeding the YAG with a narrow bandwidth seed laser allowed fine control of the wavelength of the YAG laser and also narrowed the spectrum to a few hundred MHz.

3.0 Technical Objectives

Several key features of an optically pumped systems must be demonstrated in this Phase I that prove the viability of these concepts. These are pump source frequency control, optical coupling efficiency into the molecular system, and the molecular physics associated with lasing and competing kinetic processes. We propose to use Nd:YAG pumping on the HBr (3,0) transition at 1.34 microns with lasing at 4 microns to examine these issues and to build a prototype 0.1 J laser. In this regard, the Nd:YAG pumped HBr laser system will serve as a test-bed for proving the technology essential for building both mid infrared and shorter wavelength, diode and fiber laser pumped molecular systems.

The technical objectives of Phase I are:

a. Development of a 0.1 J per pulse, efficient 1.3 μm Nd:YAG pumped laser complete with a model that describes laser performance and is validated experimentally.
b. Apply the Nd:YAG results to modeling and analysis of advanced diode and fiber laser pumped molecular systems including the H-X, alkali and interalkalai metal dimer, halogen and interhalogen molecular families. Trade-off the capabilities, scaling potential, and technical risks of these systems and identify the best system for design of a demonsrtation laser.
c. Develop a conceptual design of a 1 kW, demonstration laser using the selected fiber or diode pumped molecular laser concept. This design will be accompanied by a model that predicts laser performance.

4.0 Results

The key issues for efficient energy transfer from the Nd:YAG to the HBr is the frequency tuning and narrowing of the pump. Our approach is a two-step process. First, the Nd:YAG will be tuned by adjusting the temperature of the laser head and its lasing bandwidth will be narrowed using a combination of passive intracavity elements (prism and etalons). It is to be explored if frequency stability and purity in combination with high pulse energies are sufficient to pump HBr efficiently. Second, the Nd:YAG laser will be seeded with a narrow-band diode laser, available commercially from *New Focus*, tuned to the HBr transition. In case the intrinsic frequency stability of the diode is not sufficient, this laser can be locked to the HBr absorption. If even further stability is required for high power operation, the cavity length of the YAG laser

can be actively controlled for optimum seeding efficiency. The evolution of these design features is detailed in the following sub-sections, culminating in the demonstration of an optically pumped HBr laser at 4 microns.

4.1 Nd:YAG Source Characterization

The YAG laser used in these experiments is an SEO Schwartz 1-2-3 laser. SEO Schwartz is now owned by LaserSight Technologies (407 678-9900); they still support the 1-2-3 Laser. The 1-2-3 Laser as it was originally configured was a flash lamp pumped, free-running YAG laser with a simple linear cavity. The cavity mirrors have high reflectivity in the 1.3 μm region and low reflectivity in the 1 μm region to suppress the high gain 1.064 μm line and allow operation on the 1.3 μm transitions.

Measurements of the Nd:YAG fluorescence were made to help determine the best line in the 1.3 μm region to use for pumping HBr. These transitions are the $^4F_{3/2} \rightarrow {}^4I_{13/2}$ in Nd. The cavity mirrors were removed, and the fluorescence was collected with a lens ($f \approx 10$cm) and propagated to the Jarrel-Ash 2 m monochromator. Using narrow band-width diode lasers at 1.32 μm the resolution of this monochromator was measured to be approximately 0.5 angstrom. Because of the single shot nature of the Nd:YAG laser, the signal out of the monochromator was measured with an InGaAs photodiode (terminated into one MOhm), and averaged using a lockin amplifier with a time constant of one second. The measured fluorescence is plotted in Figure 4. The labeling of the lines is taken from Kaminskii [1]. These fluorescence lines also allow for calibrating the monochrometer at 1.3 μm. The difficulty with these labels is that the published values for these lines can vary by as much as 3 angstroms from reference to reference. In addition, a significant amount of recoil in the mechanical rotation of the monochrometer grating meant that the wavelength measurements from the monochrometer had an uncertainty of as much as an angstrom. Therefore, for detailed measurements of the lasing wavelength, we use absorption spectroscopy of HBr with a narrow-band diode laser.

A higher resolution measurement of the Nd:YAG fluorescence in region of 1.34 μm is plotted in Figure 5, along with the absorption due to the $v = 0 \rightarrow 3$ transition of HBr. Only the R branch of this transition is plotted. The plot includes absorptions due to both isotopes of HBr, $H^{79}Br$ and $H^{81}Br$. The lower wavelength branch belongs to the more abundant isotope, $H^{79}Br$.

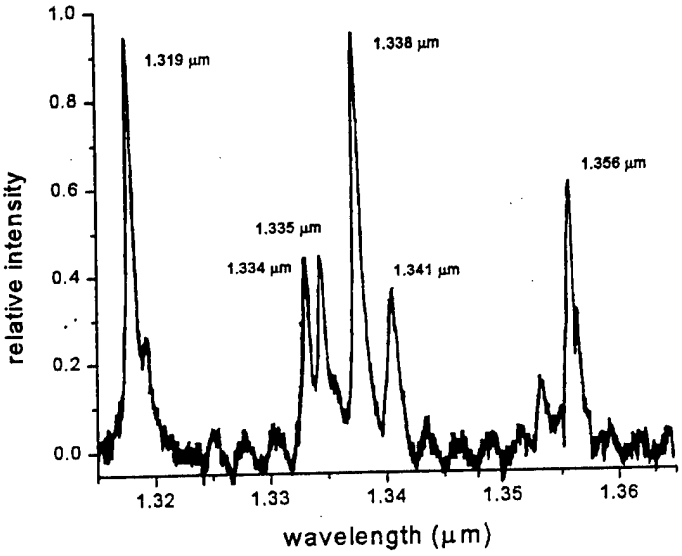

Figure 4: Nd:YAG fluorescence in the 1.3 μm region on $^4F_{3/2} - {}^4I_{13/2}$

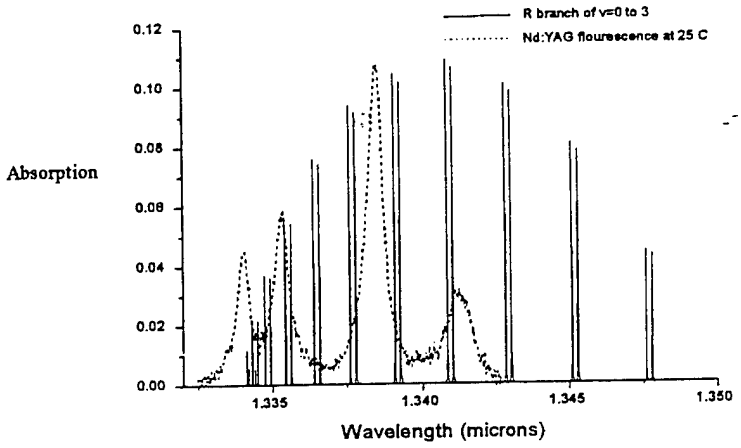

Figure 5: Nd:YAG fluorescence in the 1.34 μm region, overlaid with the R-branch transitions of HBr (calculated from Hitran).

For reference, the wavelengths of the HBr transitions are tabulated in Table 1 along with other overtone transitions.

From Figure 5, one can see a number of promising possibilities for pumping HBr. We chose the 1.338 μm transition because it is the strongest in the region, although the transitions at 1.335

μm and 1.341 μm lie closer to HBr absorptions. The 1.338 μm transition also has the advantage of being near the peak of the R branch.

4.2 Frequency Tuning of the Nd:YAG

In order to force the YAG laser to operate on a particular transition, a dispersive element is required. Our first attempts made use of intra-cavity sapphire prisms. The laser spectrum for two different alignments of the prism is shown in Figure 6. Even with two prisms in the cavity, operation on a single transition proved difficult. Operation on all the transitions in Figure 4 was observed; with the use of an additional intra-cavity etalon, consisting of a 200 μm thick microscope cover glass slide, suppressing all but a single transition. However, energy in this configuration was low (a few mJ). Furthermore, no tunability away from the peak of the transition was observed. An estimate of the linewidth expected with two intra-cavity sapphire prisms yields approximately 20 GHz.

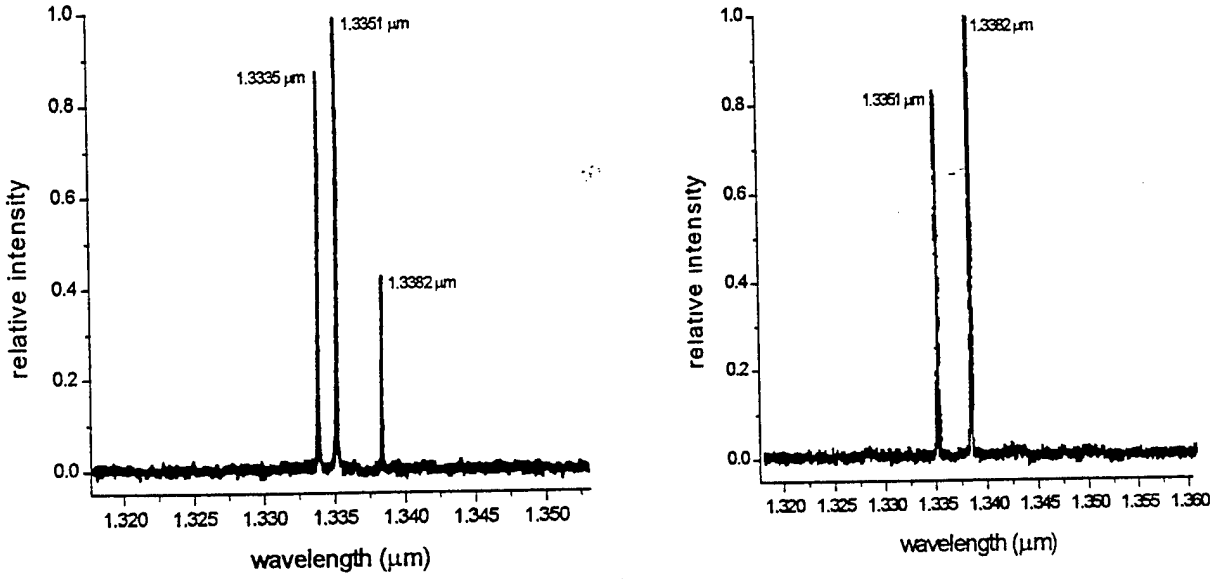

Figure 6: Spectrum of the YAG laser with intra-cavity prism.

An interesting aspect of operating the YAG laser at different frequencies is that the YAG laser emits a distinct, popping sound when oscillating on the 1.356 μm transition. This sound can not be localized to a single optical element, but is heard along the length of the laser

resonator. A high resolution scan of the Nd:YAG fluorescence around 1.356 μm is shown in Figure 7 and illustrates the dips in the fluorescence profile around 1.357 μm and 1.355 μm. These match with water absorptions in the atmosphere (as calculated by HiTran).

A). B).

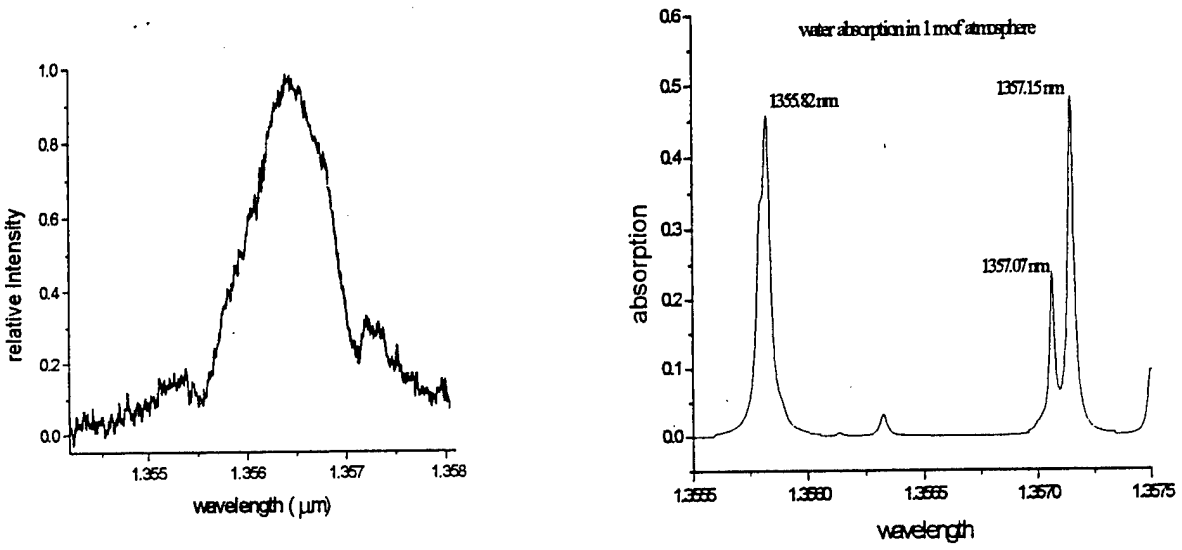

Figure 7: A). Nd:YAG fluorescence of the 1.356 μm line. B). Atmospheric absorptions.

Because the peak of the Nd:YAG fluorescence does not lie at an HBr absorption, we used temperature tuning of the YAG crystal. The fluorescence peak moves to longer wavelengths when the YAG crystal is heated. The spectrum of the YAG laser was measured using a scanning Fabry-Perot interferometer. The Fabry-Perot used flat, high-reflective mirrors designed for an iodine laser (1.315 μm). Again, because of the pulsed nature of the YAG laser, the signal, measured by an Anomalies photodiode terminated into 1 MOhm, was averaged using a lock-in amplifier. The averaging time was approximately 1 s, meaning the ramp time of the Fabry-Perot had to be much longer than one second. Typically, the ramp time was set to 60 s or greater. The free spectral range of the Fabry-Perot was estimated by measuring the distance between the mirrors. With the Fabry-Perot mirrors spaced by 1.5 mm this gives a FSR for the interferometer of 100 GHz and a resolution of 300 MHz (assuming a nominal reflectivity of 0.99 at 1.338 μm). In such a setup, the resolution will be primarily limited by the ramp time

versus the averaging time of the lock-in. For a ramp that scans the full free-spectral-range of the Fabry-Perot in one minute, the interferometer scans over 1.5 GHz during the averaging time of the lock-in amplifier.

The YAG laser was operated without etalons or prisms in the cavity to avoid affecting the spectrum due to intra-cavity dispersive elements. Under such conditions, the YAG laser operates simultaneously on both the 1.319 μm and 1.338 μm transitions. The chiller temperature was adjusted, and the system was allowed to come to equilibrium by monitoring the shift in the laser spectrum. Typically it took 10-15 minutes for the system to stabilize after adjusting the chiller temperature by 5 degrees. A plot of the spectrum (as measured by the Fabry-Perot) for different chiller temperatures is shown in Figure 8A (only the 1.338 μm line is shown, for clarity), with a linear fit to the positions of the peaks shown in Figure 8B. The linear fit gives a tuning of 1.3 GHz/°C. This can be compared to measurements of the shift in the peak of the fluorescence using the monochrometer, which returns a value of 1.8 GHz/°C. Measurement of the width of the spectrum in Figure 8 yields 10 GHz, as compared to a fluorescence line width of 125 GHz (from Figure 5). In addition to the shift in lasing wavelength in Figure 8, regularly spaced dips in the spectrum can be observed. Originally, these were attributed to atmospheric water absorptions, however there are not enough lines in the region to account for all the dips in the spectrum It was determined that these dips are due to etalon effects from the flat-flat outcoupling mirror, even though the back surface was AR coated. A wedged outcoupler did not show these effects, however currently the only outcoupler with appropriate reflectivity for Q-switching is flat-flat, and shows these etalon affects.

A narrow bandwidth external cavity diode laser was used to measure the absorption spectrum of HBr (Figure 9). (The bandwidth of the diode laser is quoted as 200 kHz by Newport.) Two photodiodes, one at the entrance to the cell, and one at the exit, were used to divide out intensity fluctuations. The HBr cell was one meter long, and the pressure was 100 torr. This measured absorption spectrum can be compared to the calculated one in Figure 5. The values for the wavelengths of the transitions (from Table 1) were then used as an absolute calibration of the wavelength of the diode laser.

Rather then using prisms, we switched to using intra-cavity etalons to select the laser transition. Initially we found that an uncoated microscope cover-glass slide (≈ 200μm thick) is

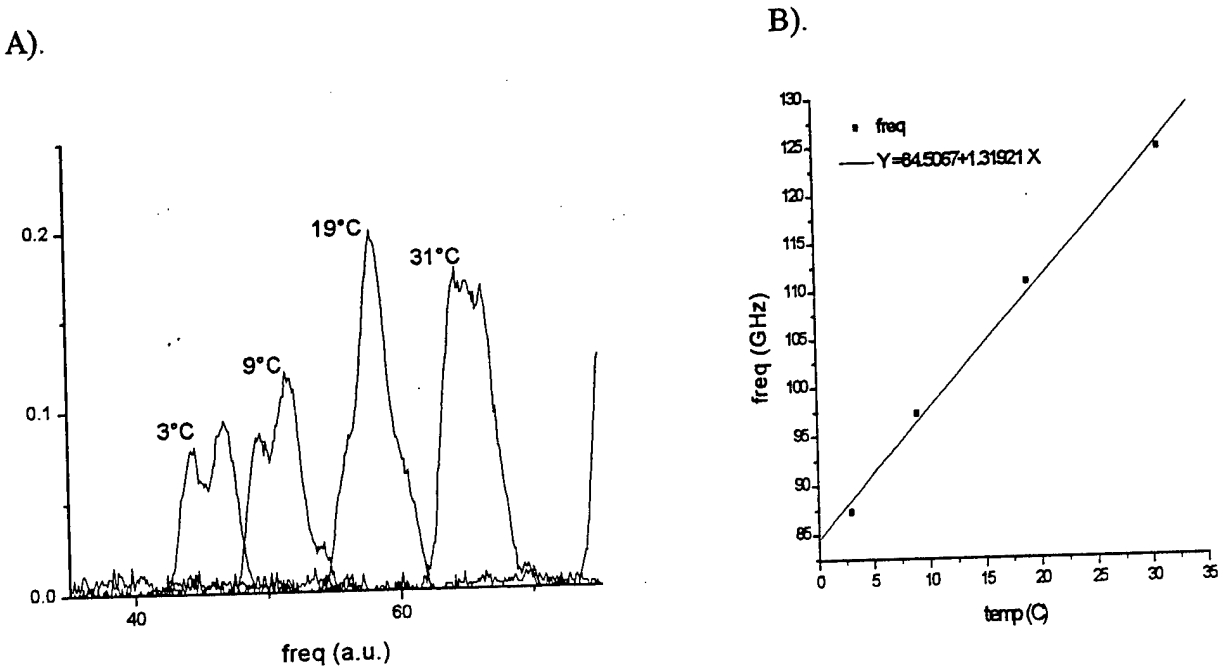

Figure 8: A). Spectrum of the Nd:YAG laser operating on the 1.338 μm line as a function of chiller temperature, (measured by the Fabry-Perot interferometer). B). Linear fit to the frequency of the peak of the spectrum.

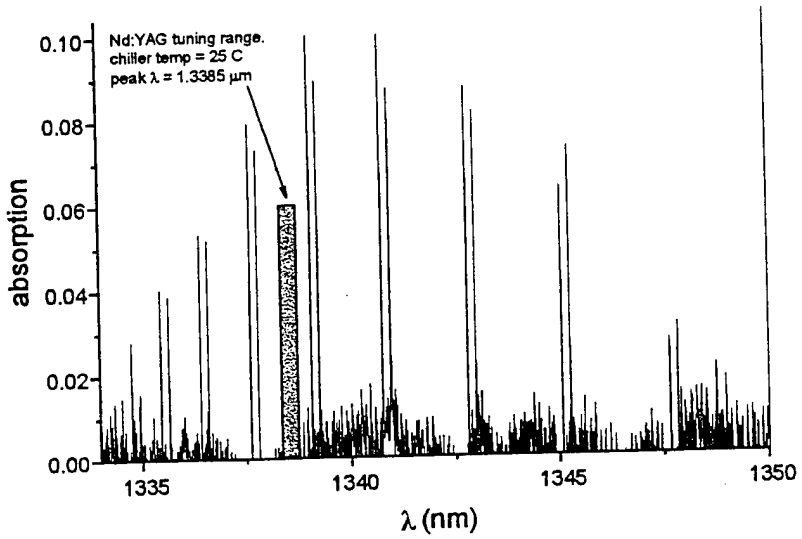

Figure 9: Absorption spectroscopy measurement of the R-branch of the $v = 0 \rightarrow 3$ of the HBr transition. The solid gray region shows the measured tuning range of the Nd:YAG laser with the coolant temperature at 25 C.

sufficient to select either the 1.338 μm or the 1.319 μm transition. Bouncing the beam off a diffraction grating at grazing incidence is a quick way to determine the lasing transition without having to resort to the monochromator. A thin (≈ 100μm) coated etalon gives more selectivity, allowing for single line lasing on the 1.319, 1.335, 1.338, and 1.356 μm transitions. A thick, uncoated etalon was inserted into the cavity as well, to give tunability away from the center of the transition. This etalon allowed approximately 65 GHz of tunability in a single transition.

4.3 Frequency Stabilization and Line Narrowing

In order to pump these lines effectively, the pump source must have the same or narrower linewidth and exhibit stable frequency operation. Since a Q-switched Nd:YAG laser operates with a width of 10 GHz, the pump laser must be narrowed. We chose the technique of injection seeding to narrow the linewidth of the YAG laser to 100 MHz. Thus, to stabilize the frequency of the YAG laser as well as narrow its bandwidth to the order of a hundred MHz, the YAG laser was injection seeded with the diode laser. A schematic of the injection seeded YAG laser with intra-cavity etalons, as it is currently set up, is shown in Figure 10.

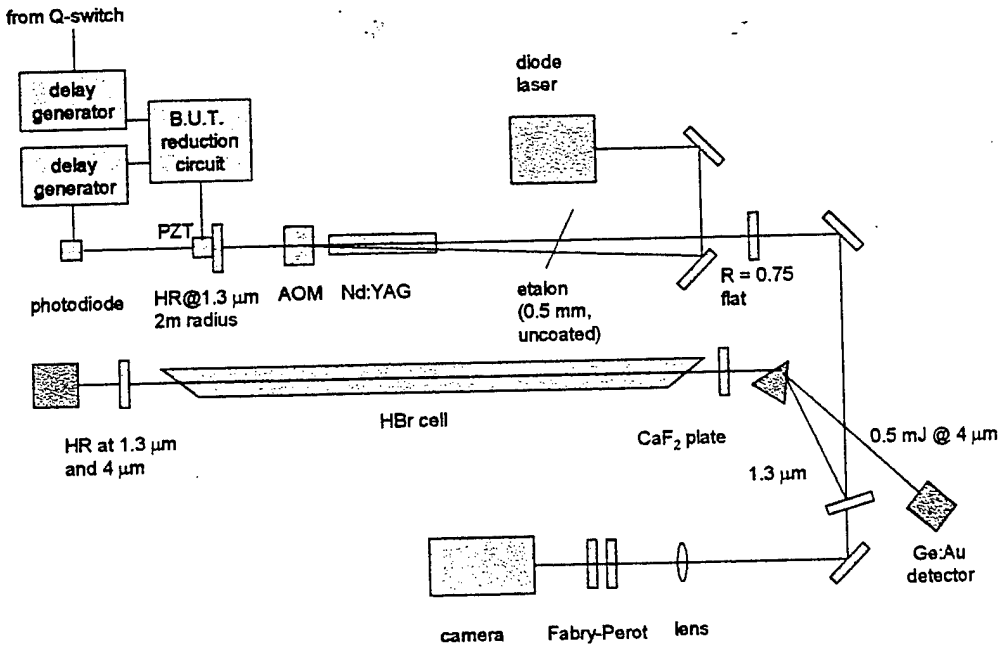

Figure 10: Schematic of the Q-switched, injection seeded YAG laser pumping the HBr cell.

The Nd:YAG cavity is linear, consisting of a high reflector at 1.34 μm with a 2 m radius of curvature and a flat outcoupler with 75% reflectivity. This gives a TEM_{00} beam radius of 0.65 mm at the outcoupler, The cavity is approximately 1.1 m long; a long cavity was used in order to increase the size of the TEM_{00} mode as much as possible. Much longer, and the cavity becomes unstable and pulse energies begin to decrease. However, the small mode volume means that much of the energy in the YAG rod remains unused.

The laser is acousto-optically Q-switched. The AOM driver takes a trigger signal from the YAG power supply. An example of a Q-switched YAG pulse is in Figure 11, showing typical longitudinal mode beating when the laser is unseeded. The YAG flashlamps axe typically run below their maximum level to avoid damaging coatings when the laser is operated in Q-switched mode. The flashlamps can be run as high as 720 V, but when Q-switched, we generally keep the flashlamps below 600 V. At 575 V, the laser puts out approximately 30 mJ per pulse (in TEM_{00} mode). The diode laser can be aligned by decreasing the drive amplitude of the AOM until the cavity hold-off is no longer sufficient to prevent pre-lasing. This allows a small amount of YAG laser radiation to propagate back along the first diffraction order, and the diode laser can be aligned to be co-linear with the YAG along the first diffraction order. Care must be taken in order to prevent the pre-lasing YAG pulse from propagating back to the diode laser.

An example of a Q-switched pulse when the YAG is injection seeded is shown in Figure 11. In contrast to the unseeded pulse, the seeded pulse shows a smooth profile. The lack of mode-beating means that the laser is operating on a single longitudinal mode, and it's bandwidth is less than that of the free-spectral range of the cavity, or 100 MHz.

The injection seeding works as follows: as long as the AOM is on, and the YAG laser is prevented from lasing, seed light from the diode laser is continuously injected into the cavity. When the flash lamps are through firing, and the AOM turns off, seed light is no longer injected into the cavity. The YAG laser begins to build up on the one round trips worth of seed light that is left in the YAG cavity. The Newport diode laser puts out 4 mW at 1.34 μm. Of this, 0.64 mW is injected into the YAG resonator, sufficient to seed the laser.

For injection seeding to be stable, the length of the YAG cavity must be constantly adjusted so that the wavelength of the seed light matches exactly one of the longitudinal modes of the

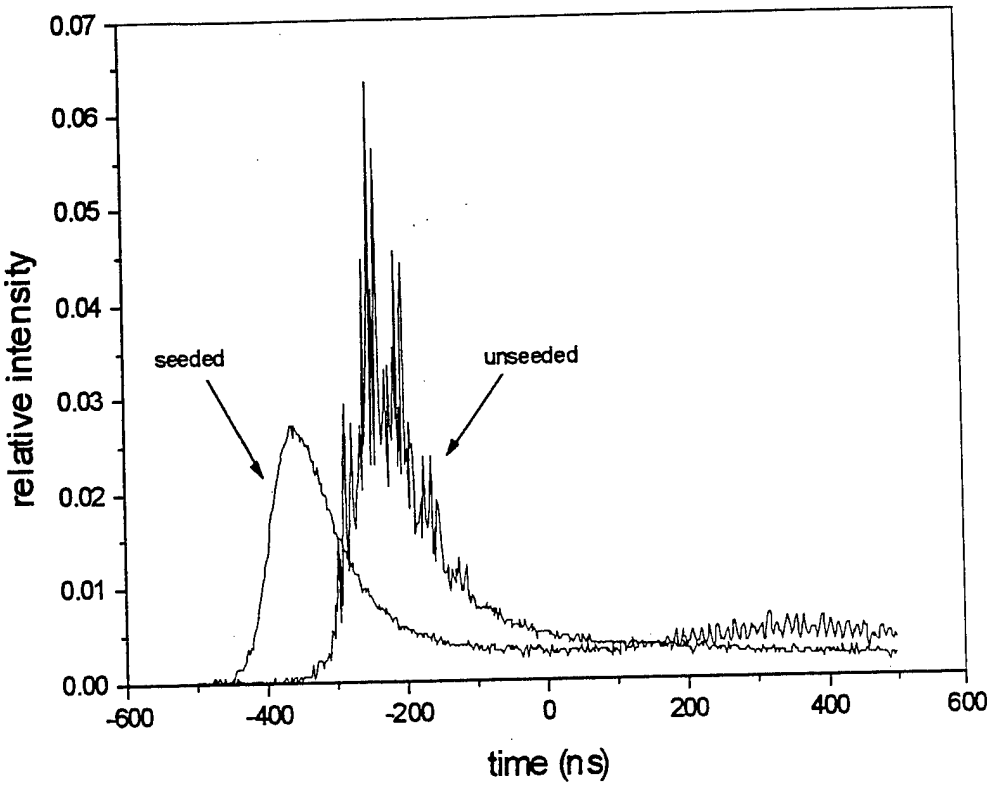

Figure 11: Injection seeded versus unseeded Q-switched Nd:YAG pulses.

YAG cavity. A standard technique for doing this is based on the concept of **build-up time reduction.** If the seed light wavelength does not match the wavelength of one of the longitudinal modes of **the YAG** cavity, the seed light is rejected from the YAG cavity. In such a case, the time between when the Q-switch is opened, and the laser pulse is observed (the build-up time of the cavity depends on the spontaneous emission rate of the Nd:YAG rod, i.e. the length of time to build up a laser pulse from noise).

If however, the seed and the YAG cavity wavelengths match exactly, seed light builds up inside the YAG cavity. When the Q-switch is opened in this case, there are a significant number of photons in the cavity. Since the YAG laser does not start from noise, but rather from the seed photons, the build-up time of the cavity is significantly reduced. For this laser, the seeded YAG pulse has a build up time shorter by almost 200 ns then in the case of the unseeded pulse (Figure 11).

One of the end mirrors of the cavity is mounted on a PZT (A Burleigh model PZ-80). The build up time is measured by an electronic circuit that takes a trigger from the AOM and a

signal from a photodiode that detects the laser pulse. The circuit drives the PZT in such a way as to find the minimum of the build-up time of the cavity. We use a circuit based on a design for a commercial Spectra Physics CCR YAG laser, injection seeded by a Lightwave diode pumped, CW YAG laser. The circuit diagram, for reference purposes, is shown in Figure B-1 and Figure B-2 in Appendix B.

Because this circuit is designed for a different laser, it expects the build up time to fall within a certain range. If the time between Q-switch and laser pulse falls outside the range that the circuit can handle, the circuit will fail to measure the build-up time properly. For this reason, we use variable delay generators to condition the pulse from the Q-switch and the photodiode for the build-up time reduction circuit (The circuit has 50 Ohm input impedance). The circuit puts out a diagnostic voltage proportional to the measured build up time. If the build up time is too long or too short, the diagnostic voltage will rail at its high ($\approx$ 12 V) or low ($\approx$ 2 V) value. Incidentally, this diagnostic voltage is ideal for fine tuning the alignment of the seed laser into the YAG cavity. The input mirror is adjusted such that the build up time (i.e. the diagnostic voltage) is a minimum value.

The center wavelength of the laser was measured to be 1.3385 μm. This is measured by first calibrating the diode laser using the absorptions shown in Figure 9 and comparing them to the values in Table 1. The laser is injection seeded and sent to the single-shot Fabry-Perot interferometer. The seed laser frequency can then be tuned to the YAG frequency by blocking and then unblocking the seed laser. If there is a frequency difference between the seed laser and the YAG laser, the size of the fringes from the seeded laser are different then those of the unseeded laser. By tuning the seed laser to the center of the YAG spectrum, one can precisely measure the YAG wavelength.

4.4 HBr Laser Oscillation

In order to pump the HBr, the diode laser is tuned to the R(4) transition of the ^{79}Br isotope at 1.33909 μm. The coolant temperature is set to 85 C. Given that the measured temperature tuning of the YAG was between 1.3 and 1.8 GHz/C, and the YAG wavelength is 1.3385 μm at a coolant temperature of 25 C, we would expect the center of the transition to reach 1.33909 μm at a coolant temperature between 79 and 100 C. We begin to observe injection seeding at 1.33909 μm at a coolant temperature of approximately 70 C at the edge of the long wavelength side of the tunability range. Alternatively, given the measured center wavelengths and

temperature tuning, the coolant temperature would have to be between -40 and -64 C to reach the 1.33781 μm line of the ^{81}Br isotope.

The HBr cell is approximately 1 m long. It has CaF2 windows, as well as a side port with CaF2 windows for observing side fluorescence. With 50 torr HBr in the cell and the YAG laser injection seeded at the HBr absorption wavelength side, fluorescence is observed using a liquid nitrogen cooled, Mercad-Telluride detector (Figure 12). The detector uses long wavelength pass filters to reject any of the scattered pump radiation. The fluorescence signal is passed by a wavelength filter that has a cut-on at 3.4 μm but is blocked by any amount of BK7 glass or fused silica (these glasses start absorbing around 2 μm.). When the YAG is injection seeded and the fluorescence is present, the HBr pressure, measured by a baratron, is observed to increase by a few millitorr. In addition an audible sound can be heard at high pump energies. Acoustic signals have been used in other experiments to detect narrow molecular absorptions in gases. This small pressure jump is the signal we typically use while tuning the seed laser frequency in order to find the HBr absorption.

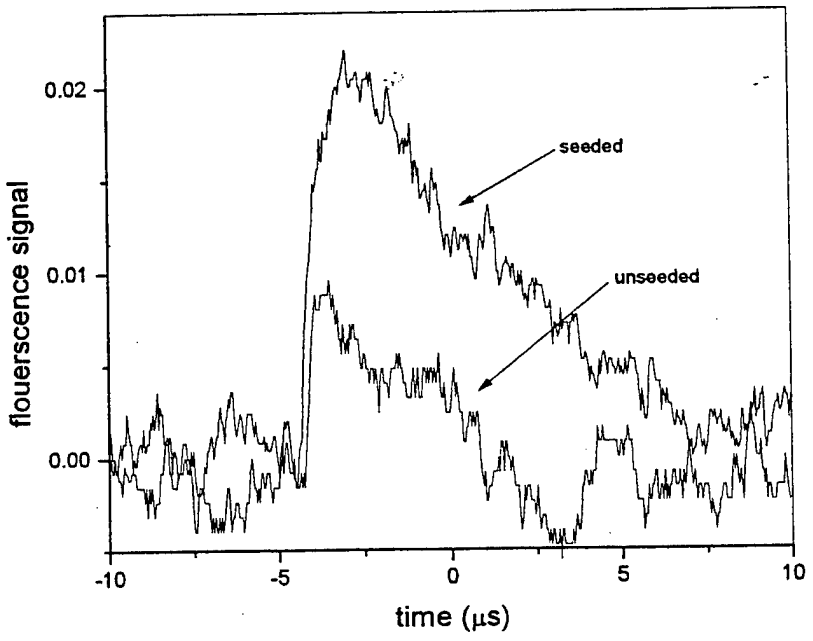

Figure 12: Side fluorescence of HBr at 4 microns when the Nd:YAG is seeded versus unseeded.

A 4 μm resonator was then built around the HBr cell. One end mirror was flat, with approximately 80% reflectivity at 4 μm and also highly reflective at 1.34 μm allowing us to double pass the pump. The other end mirror was a flat, uncoated CaF2 plate. On the input side of the cell, the pump entered through a sapphire prism, allowing us to separate the 1.34 μm and 4 μm beam. Four micron pulses were measured with a liquid nitrogen cooled, gold doped, germanium detector that, although noisy, allowed us to time-resolve the HBr laser pulses. Examples of HBr laser pulses at two different frequencies are shown in Figure 13. HBr lasing is only observed when the YAG laser is seeded. The HBr pressure was measured with a baratron, however the baratron was damaged, so the pressures quoted in Figure 13 are only rough estimates. Output pulse energy was approximately 0.5 mJ. Most likely the low output energy is due to the low Q of the HBr cavity and the flat-flat mirrors used for the HBr resonator. Although the detector is noisy, one can see that the pulse width is much shorter at high gas pressure, and at low pressure, the pulse contains significant structure, possibly due to cascade lasing at low pressures. The short duration of the pulses is again most likely due to the low Q cavity. Lasing was erratic because of fluctuations in the seeding of the YAG laser. Lasing is only observed when the YAG laser runs single longitudinal mode. For this reason, the next step is to rebuild the YAG laser for more stable operation.

More recently, a stable 4 μm cavity has been built using a high reflector at 4 μm with a 5 m radius of curvature at the position of the gold doped germanium detector in Figure 10. The mirror was aligned by first obtaining lasing with the CaF_2 end mirror, and then adjusting the alignment of the high reflector until the signal on the Mercad-Telluride detector increased. This stable cavity significantly lowered the lasing threshold and increased the stability of the 4 μm laser.

5.0 Summary and Conclusions

The v = 0 →3 transition of HBr has been successfully pumped by an injection seeded, Nd:YAG laser operating at 1.3391 μm with subsequent laser oscillation at 4 μm. In accomplishing this task, several important design criteria were evolved and developed that enabled the laser to operate. These include the ability to narrow-band and frequency shift the pump source and the ability to efficiently couple pump energy into the lasing species. The critical techniques for narrow-lining the optical source, temperature tuning and stabilizing the output frequency of the optical source; the efficient coupling of optical energy into the

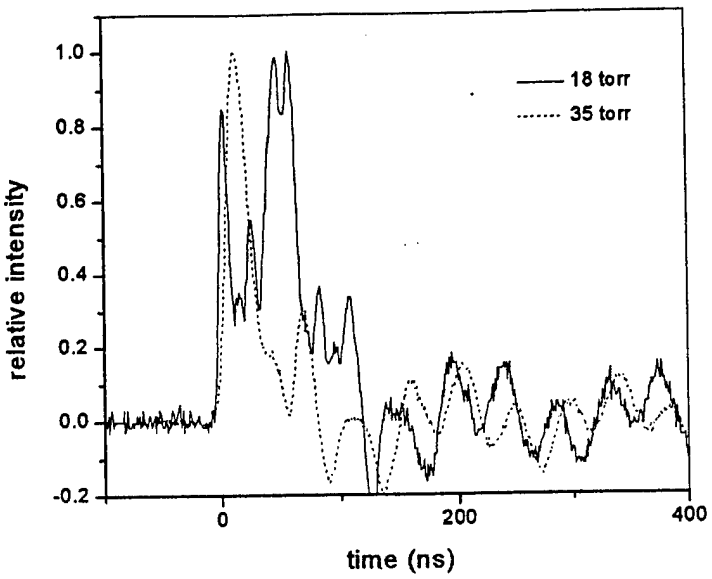

Figure 13: 4 μm laser pulses as a function of HBr pressure.

molecular laser; and the efficient optical extraction from the lasing molecule have been demonstrated. In addition, work to date has concentrated on high resolution spectroscopy of the HBr and Nd:YAG laser to ensure that the pump source can be made to overlap an HBr absorption. The Nd:YAG is forced to operate in the 1.3 μm region with dielectric mirrors that have a high reflectivity at 1.3 μm and low reflectivity at 1.064 μm. Course frequency tuning of the Nd:YAG is provided through temperature control of the YAG rod. The 1.34 μm line is selected using intracavity etalons, and fine frequency control/ bandwidth narrowing is provided by injection seeding from a narrow linewidth tunable diode laser.

Future work in the development of an optically pumped HBr laser will focus on stabilizing the seed laser and enhancing the energy output of the device. A detailed design for addressing these issues has been advanced. Included among the projected steps to enhance the performance of the device are locking the diode seed laser to an HBr absorption cell, optimize the temperature tuning of the Nd:YAG rod, increasing the length of the cell, refine the HBr resonator and vary the HBr and diluent pressure and temperature. Furthermore, additional power extraction is advocated by means of coupling auxiliary amplifiers to the Nd:YAG oscillator. Figure 14 outlines these steps and illustrates the preliminary design features and components for scaling the optically pumped HBr laser to high powers.

Proposed Design Features to Enhance HBr Laser Performance

1. Lock diode seed laser to HBr cell (work in progress)
2. Measure spectrum of 4-μm HBr laser emission
3. Optimize current low-energy set-up
   a. optimize Nd:YAG temperature
   b. vary HBr and diluent pressure
   c. increase length of cell
   d. optimize HBr resonator
   e. chill HBr cell
   f. use isotopically enriched HBr
4. *Scale pump laser by means of adding amplifiers*

High Energy Pump Laser Concept:

Addition of Auxiliary Power Amplifiers

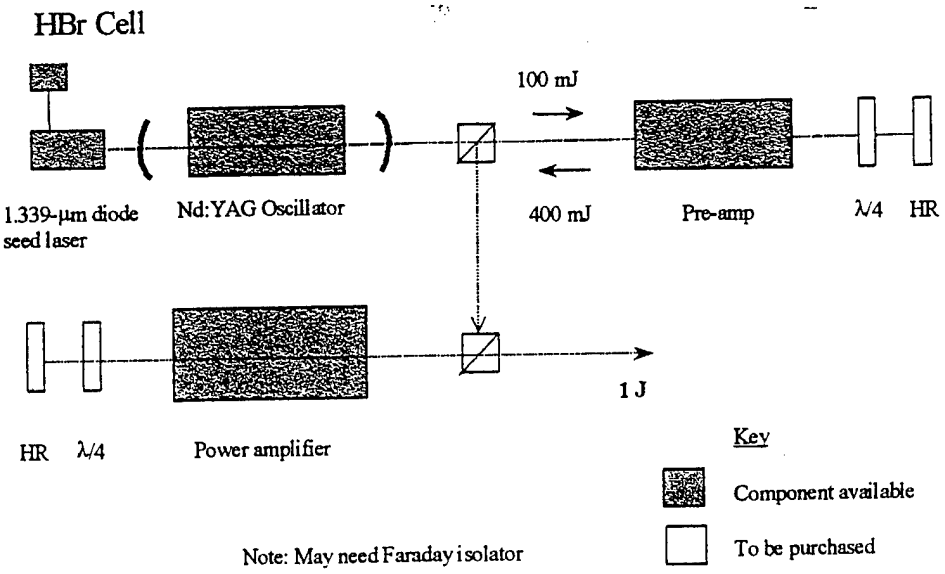

Figure 14. Design Steps, Features and Components for Enhancing the HBr Laser Performance.

References

[1] A. Kaminskii. *Laser Crystals : Physics and Properties.* Springer-Verlag, Berlin, 1981.

[21 H.J. Babrov, "Strengths and self-broadened widths of the lines of the hydrogen bromide fundamental band." *Journal of Chemical Physics*, 40(3):831-837, 1964.

[3] R.N. Stocker and A. Goldman, *J. Quant Spectrosc.* Radiat. Transfer, 16:335, 1976.

[4] H.C. Miller, D.T. Radzykewycz, and G. Hager. "An optically pumped mid-infrared HBr laser." *IEEE Journal of Quantum Electronics*, 30(10):2395-2400, 1994.

[5] P. Bernage and P. Niay, "Absorption intensities for vibration-rotation bands and the dipole moment expansion of HBr," *J. Quant. Spectrosc. Radiat. Transfer*, 18:315-325, 1977.

[6] P. Bernage and P. Niay, "Absorption intensity for vibration-rotation bands and the dipole moment expansion of HBr : Erratum," *J. Quant. Spectrosc. Radiat. Transfer*, 25:95, 1981.

[7] N. Nishimiya, T. Yukiya, T. Ohtsuka, and M. Suzuki, "Laser spectroscopy of vibration-rotation lines in the 3-0, 5-0 and 6-0 overtones of HBr," *Journal of Molecular Spectroscopy*, 182:309-314, 1997.

[8] T.F. Deutsch, "New infrared laser transitions in HCI, HBr, DCl, and DBr," *IEEE Journal of Quantum Electronics*, pages 419-421, 1967.

Appendix A. HBr Data

Table A-1: Some physical and spectroscopic data of HBr [4-8].

$v = 0 \rightarrow 2$		$v = 0 \rightarrow 3$		$v = 0 \rightarrow 4$	
λ (μm)	abs	λ (μm)	abs	λ (μm)	abs
1.9371	0.01277	1.33413	0.01103	1.02471	0.04089
1.93738	0.01255	1.33428	0.02054	1.0249	0.07457
1.93785	0.03527	1.33448	0.02013	1.02529	0.04486
1.93814	0.03463	1.33472	0.03454	1.02586	0.04972
1.93898	0.08673	1.33492	0.03382	1.02663	0.0494
1.93927	0.08519	1.33546	0.05621	1.02759	0.04261
1.94049	0.1904	1.3356	0.05505	1.02778	0.04159
1.94078	0.1871	1.33639	0.07821	1.02874	0.03208
1.94238	0.3537	1.33658	0.0766	1.02893	0.03131
1.94267	0.3479	1.33762	0.09583	1.03019	0.01441
1.94475	0.5519	1.33781	0.09371	1.03348	0.01288
1.94504	0.5441	1.33909	0.1053	1.03367	0.01253
1.94741	0.7381	1.33929	0.1029	1.03553	0.02561
1.9477	0.7303	1.34082	0.1039	1.03768	0.03043
1.95046	0.8916	1.34102	0.1015	1.03787	0.02971
1.95075	0.8859	1.3428	0.08911	1.04013	0.03164
1.9539	0.9557	1.343	0.08692	1.0427	0.02847
1.95419	0.9523	1.34508	0.06734	1.04548	0.02287
1.95774	0.9785	1.34528	0.06566	1.04567	0.02237
1.95802	0.9764	1.34762	0.02995	1.04857	0.01646
1.96197	0.9857	1.34782	0.02918	1.05178	0.01046
1.96226	0.9841	1.35344	0.02655	1.05198	0.01025
1.96662	0.9854	1.35364	0.02586	1.05532	0.00575
1.96691	0.9837	1.35677	0.05315		
1.97167	0.9739	1.35692	0.0518		
1.97197	0.9713	1.36037	0.06269		
1.97705	0.9389	1.36055	0.06116		
1.97734	0.9343	1.36425	0.0652		
1.98285	0.7093	1.3644	0.06367		
1.98314	0.6995	1.36835	0.05876		
1.99575	0.6927	1.36856	0.05747		
1.99605	0.6828	1.37279	0.04749		
2.00276	0.9218	1.373	0.04642		
2.00307	0.9164	1.37747	0.03434		
2.01024	0.9581	1.37768	0.03359		
2.01054	0.9545	1.3825	0.0218		
2.01817	0.9703	1.38266	0.02133		
2.01848	0.9675	1.38777	0.0118		
2.02648	0.9659	1.38793	0.01156		
2.02679	0.9629	1.39335	0.00622		
2.03527	0.9461	1.39351	0.00609		
2.04434	0.8966				
2.04466	0.891				
2.05403	0.7877				
2.05435	0.78				
2.06413	0.591				
2.06445	0.5828				
2.07476	0.4016				
2.08572	0.235				
2.08605	0.2308				
2.09724	0.117				
2.09757	0.1149				

Doppler linewidth at 300 K	400 MHz
Pressure broadening coefficient	10 MHz/Torr
$v = 0 \rightarrow 3$ abs. cross section	2×10^{-20} cm^2
$v = 1 \rightarrow 0$ s.e. cross section	2.5×10^{-18} cm^2
anharmonicity constant, χ_e	0.0171
ω_e	2649.1 cm^{-1}
rotational constant	2.546×10^{11} s^{-1}
moment of inertia	3.298×10^{-47}kg m^2
approx. separation of rotational transitions	0.5 THz
approx. isotopic separation	40 GHz
isotopic abundance	^{79}Br = 50.5% ^{81}Br = 49.5%
Gain on $v = 3 \rightarrow 2$ transition after pump pump : 30 mJ, 1 mm diameter HBr : 1 m cell, 50 Torr	0.1 cm^{-1}

Appendix B. Control Circuits

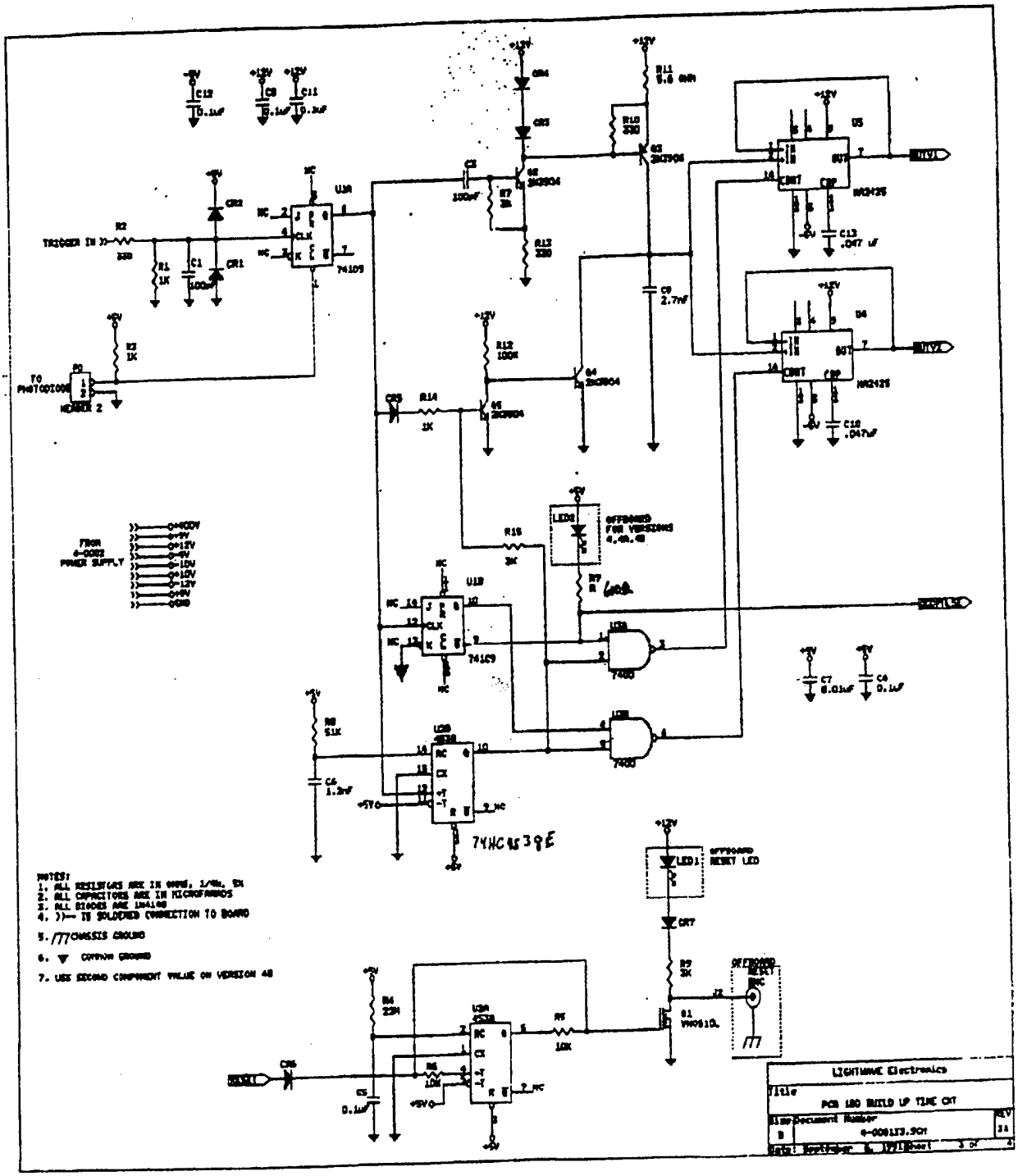

Figure B-1. Build-up time reduction circuit.

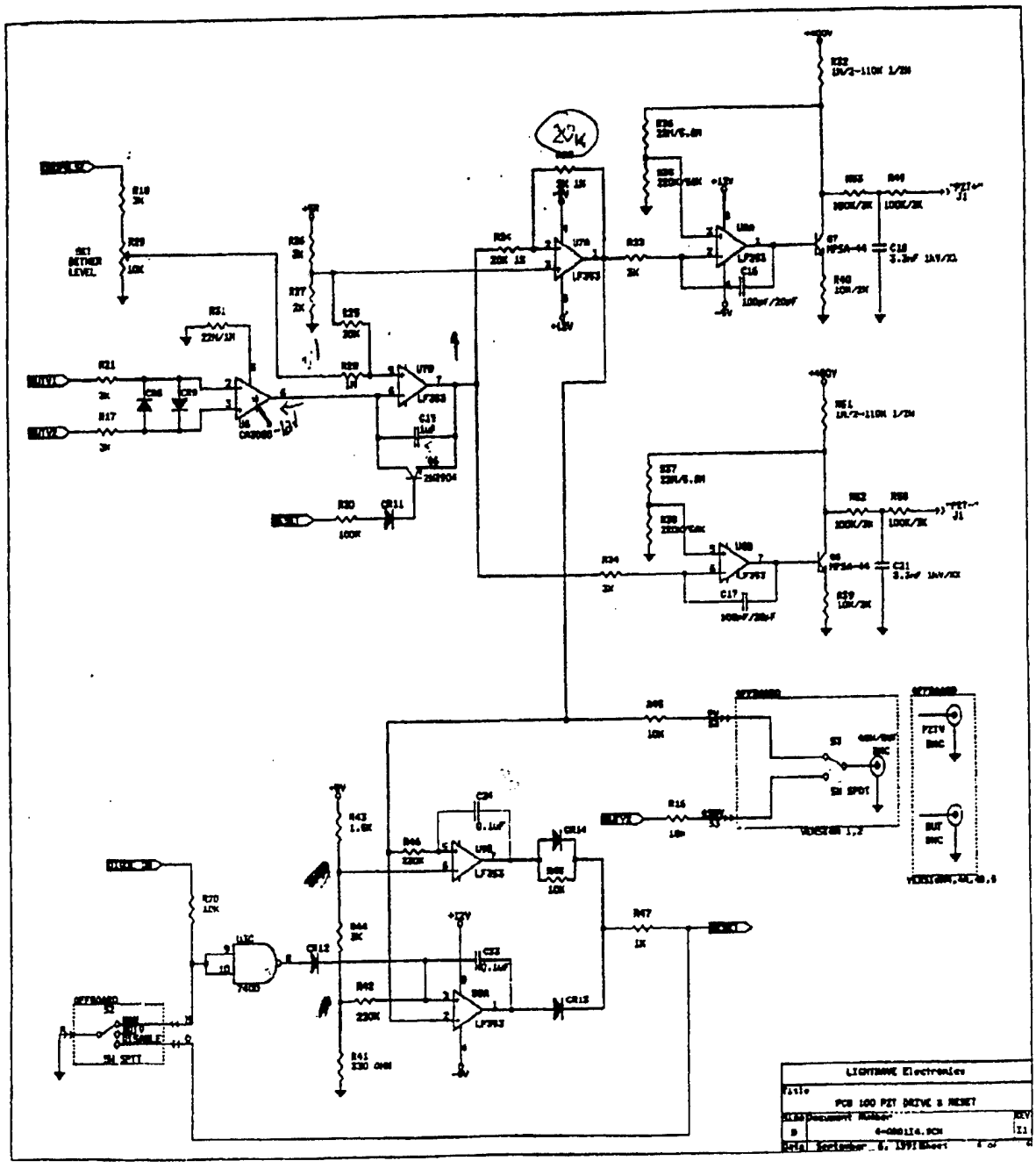

Figure B-2. Build-up time reduction circuit.

DISTRIBUTION LIST

DTIC/OCP 8725 John J. Kingman Rd, Suite 0944 Ft Belvoir, VA 22060-6218	1 cy
AFSAA/SAMI 1570 Air Force Pentagon Washington, DC 20330-1570	1 cy
AFRL/VSIL Kirtland AFB, NM 87117-5776	2 cys
AFRL/VSIH Kirtland AFB, NM 87117-5776	1 cy
Directed Energy Solutions 14125 Candlewood Ct Colorado Springs, CO 80921	1 cy
Official Record Copy AFRL/DELC/Gordon D. Hager	2 cys